Coding and Coherent Decoding Techniques for Continuous Single Slope Cyclic Shift Chirp Signal

Lerson KIRASAMUTHRANON [1], Paramote WARDKEIN [2], Jeerasuda KOSEEYAPORN [2]

[1] Dept.of Electronics Engineering Technology, College of Industrial Technology,
King Mongkut's University of Technology North Bangkok, Bangkok, Thailand 10800
[2] Dept. of Telecommunications Engineering, School of Engineering,
King Mongkut's Institute of Technology Ladkrabang, Ladkrabang, Bangkok, Thailand 10520

lersonk@kmutnb.ac.th, {paramote.wa, jeerasuda.ko}@kmitl.ac.th

Submitted November 17, 2022 / Accepted March 16, 2023 / Online first May 17, 2023

Abstract. *Chirp signals are currently widely used in broadband and spread spectrum communications due to their advantageous features, such as immunity to fading noise, low power consumption, consistent long-range transmission, and constant bandwidth. As a result, they are applied at the physical layer of the Internet-of-Things (IoT). This study proposes two techniques for encoding and decoding 4-cyclic shift chirp symbols, based on addition and subtraction operations. The proposed techniques have simple structures that can be easily implemented using analog circuits. The proposed encoding techniques reveal obviously the relationship between cyclic-shift chirp symbols and pulse modulating signals (PWM, PPM, and PAM), which is rarely discussed in prior research. Moreover, the circuit for encoding and decoding of the proposed technique is implemented by discrete commercial devices at low frequency (25–35 kHz) which is suitable for sonar and communication under water; however this proposed technique is not limited to only low frequency but is also capable of being used in high frequency band as well which experimental and simulation result show agreeing well with each other.*

Keywords

Chirp signal, chirp symbol, cyclic-shift chirp modulation and demodulation, chirp signal spectrum, chirp spread spectrum

1. Introduction

In communication systems, it is important to translate the frequency components of the original information signal to a frequency range suitable for the transmission medium or frequency multiplexing. This can be achieved through modulation, which involves the process of frequency translation. Analog modulation can be classified into two categories: angle modulation, including frequency modulation (FM), phase modulation (PM), and amplitude modulation (AM) [1]. FM is commonly used in communication systems due to its improved noise immunity compared to AM. In digital communication, FM is utilized for frequency encoding in FSK [2] and in radar systems such as FMCW [3]. For radar applications, the chirp signal, which represents frequency modulation with a linear information signal, is employed for distance and velocity measurements. This type of FM signal is referred to as a modulated chirp signal [4] and is currently used for data transmission in Lora systems [5].

The modulated chirp signal has several advantages. It provides high immunity to noise and fading signals as it is encoded in both frequency and time. It can be used for data transmission over long distances while consuming low and fixed energy per bit [6]. Based on the literature review, the encoding and decoding of chirp signals can be classified into three techniques: digital [7–10], analog [11], and hybrid. The digital technique utilizes a signal-processing procedure to produce chirp symbols. The common methods for generating chirp signals consist of two processes [8], [11]. The first process involves coding the data into chirp symbols, and the second process involves using these chirp symbols as input for frequency modulation. The resulting chirp symbol has the form of a sawtooth wave with a positive or negative slope that represents the data bits "1" and "0", respectively. This chirp symbol is then used as the input for a digital control oscillator. Alternatively, if the chirp symbol is used as the input of a voltage-controlled oscillator, it is referred to as a hybrid technique. For decoding the chirp signal, it is divided into two categories: coherent [12] and noncoherent [13–16]. The coherent technique involves multiplying the received chirp by a reference chirp symbol, while the noncoherent technique mainly relies on the fractional Fourier transform [13–16].

Cyclic-shift chirp encoding or phase modulation of the sawtooth signal was first introduced in 2013 [16] and named as cyclic-shift chirp in 2014 [17]. A notable feature of this encoding signal is that its initial and final instantaneous frequency of the chirp signal are the same. Cyclic-shift chirp modulation is widely used for data transmission, but its encoding and decoding structures are rarely discussed. Most studies on encoding process use either a VCO with a cyclic-

DOI: 10.13164/re.2023.0273

shift chirp symbol as the input, or an FPGA. In this paper, a simple structure for encoding cyclic-shift chirp signals is proposed, which can be realized through analog circuits. Additionally, two coherent decoding techniques are presented, one utilizing addition and the other subtraction operations. The decoded signal produced by these techniques is a hybrid PAM-PWM signal, offering versatility in demodulating the information signal through either PAM or PWM. The proposed encoding and decoding techniques at low frequency (25–35 kHz) band have potential applications in chirp sonar transmission and underwater communication [27].

The organization of the paper is summarized as follows: In Sec. 2, the principles of the chirp and cyclic-shift chirp signal, their relationship with pulse modulation, and the mathematical model of the cyclic-shift chirp symbol are discussed. In Sec. 3, the proposed encoding and coherent decoding techniques of the cyclic-shift chirp signal are described, as well as a frequency analysis of the signal's bandwidth and error performance analysis. Section 4 includes experimental results of real circuits and Matlab simulation results and illustrations of the spectra and error probability performance of the proposed techniques. The conclusions are presented in Sec. 5.

2. Principles

2.1 Chirp Modulation

Chirp modulation is a type of frequency modulation where the carrier frequency changes in a linear or nonlinear manner over time. In digital communication, a chirp signal can represent data bits with an increasing frequency (up-chirp) or decreasing frequency (down-chirp). In mathematics, a chirp signal can be defined as a signal with a frequency that varies linearly with time as given by

$$c(t) = A\cos\left(\omega_c t + \frac{1}{2}\mu t^2\right) \tag{1}$$

where A is the amplitude of the chirp signal (volt), ω_c is the angular frequency of the carrier signal (radian/second), μ is the chirp rate (radian/second^2). According to (1), the instantaneous frequency $\omega_i(t)$ of the chirp signal is determined by taking the derivative of the angular phase with respect to time,

$$\omega_i(t) = \omega_c + \mu t\ . \tag{2}$$

The frequency of the chirp signal is changed from low to high (up-chirp) or from high to low (down-chirp) for $\mu > 0$ and $\mu < 0$, respectively. The concept of up-chirp and down-chirp is illustrated in Fig. 1.

The bandwidth of the chirp signal can be determined by the following expression [18], [19]:

$$BW = |\mu|T = \frac{|\mu|}{R_s} \tag{3}$$

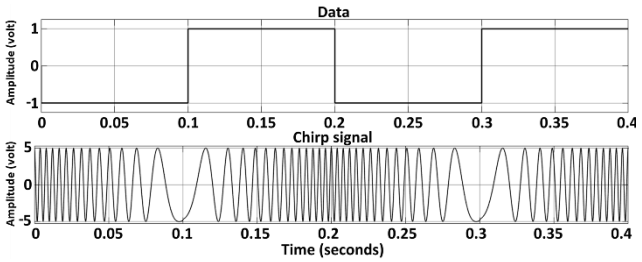

Fig. 1. Example of chirp signal.

Variable	Description
A	The amplitude of the chirp signal (volt)
ω_c	The angular frequency of the carrier signal (radian/second)
μ	The chirp rate (radian/second^2)
R_s	The symbol rate (symbol/second)
$V_p(i)$	The initial voltage level (corresponding to the initial phase) of the i^{th} symbol
T_s	The period of a cyclic-shift chirp symbol
t_{di}	The duration of the first interval of the sawtooth signal corresponding to the i^{th} chirp symbol
$S_{ch}(t)$	The chirp symbol
$s_{cp}(t)$, $s_{cn}(t)$	The positive ramp and negative ramp signals
f_c	The carrier frequency (Hz)
k_f	The sensitivity or gain of the VCO (Hz/volt)
k_v	The slope of chirp symbols (volt/second)
F_n	The exponential Fourier series coefficient
$\phi_{FM}(t)$	The frequency modulated signal
f_0	The fundamental frequency (Hz)
$\rho(s_i, s_j)$	The normalized correlation of the 4-cyclic shift chirp symbols
E_s	The energy of the cyclic-shift chirp symbol
$D^2(s_i, s_j)$	The squared Euclidean distance
P_{erf}	The Rayleigh fading probability

Tab. 1. List of variables.

where μ is the chirp rate (radian/second^2), T is the time interval for transmitting one data symbol (second), R_s is the symbol rate (symbol/second). In order to simple analysis and easy understand the various parameters are defined in Tab. 1.

2.2 Relationship between Cyclic-Shift Chirp Symbol and Pulse Modulating Signal

Currently, Lora devices play an important role in the IoT and that chirp modulation is used for data transmission in this technology [20]. In [17], a new form of bit symbols has been introduced to improve the high-speed data transmission performance. More patterns of data symbols can be generated by phase encoding of the sawtooth carrier signal, where each pattern of the data symbols has a distinct initial phase. For example, there are four patterns of data symbols for two data bits, as illustrated in Fig. 2(a). The four-bit patterns 00, 01, 10, and 11, each occupy initial phases of the sawtooth signal, respectively. The resulting cyclic-shift chirp symbol has identical initial and ending phases, called as cyclic-shift chirp symbol. When this cyclic-shift chirp

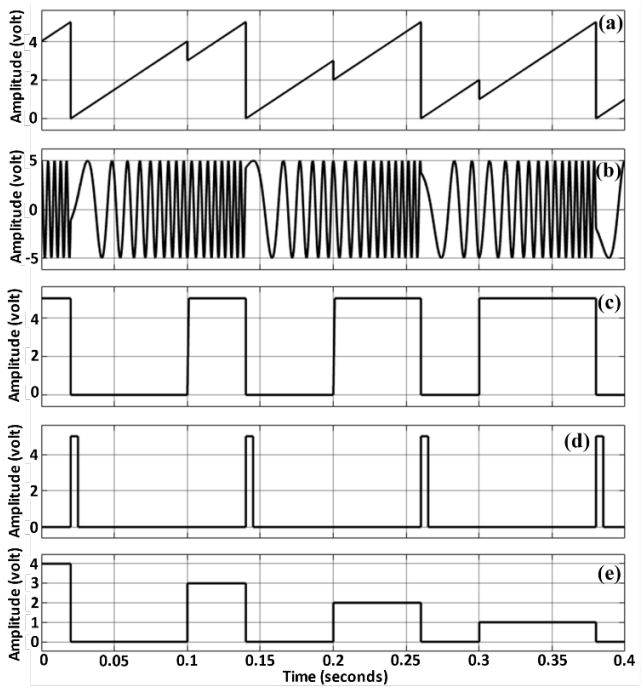

Fig. 2. Example relations between chirp symbols, chirp signal, and pulse modulating signals for encoding of two data bits.

symbol is passed through a voltage-controlled oscillator (VCO), the output is a cyclic-shift chirp signal. This process is illustrated in Fig. 2(b).

In addition, the relationship between cyclic-shift chirp symbols and pulse modulating signals (PWM, PPM, and PAM) is described. The width of the positive-pulse of the PWM signal is proportional to the voltage level of the initial phase of the cyclic-shift chirp symbol as depicted in Fig. 2(c). The PPM signal is obtained by triggering the rising edge of the PWM signal, and the PAM signal is related to the cyclic-shift chirp symbol as shown in Fig. 2(d) and 2(e), respectively. The proposed coherent decoding techniques use this relationship to transfer the information in the form of cyclic-shift chirp symbol into the form of either width of PWM signal or pulse position of PPM signal or amplitude of PAM signal, which provides flexibility in demodulating information data bits that can be retrieved from either amplitude or width of the pulse signal.

2.3 Mathematical Model Structure of Cyclic-Shift Chirp Symbol

The mathematical model of a cyclic-shift chirp symbol is discussed in this subsection. It is in the form of two intervals of a sawtooth signal and can be considered as the composition of two parallel straight lines ($L_1$and L_2), as shown in Fig. 3. The mathematical expression for the symbol is given in terms of its lower and upper bounds along the x and y-axis, which are [x_o, x_{max}] and [y_{min}, y_{max}], respectively. The mathematical expression is given by

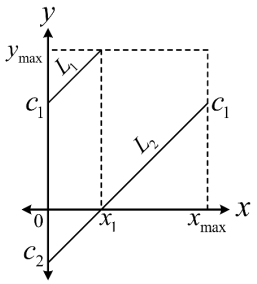

Fig. 3. Model of cyclic-shift chirp symbol.

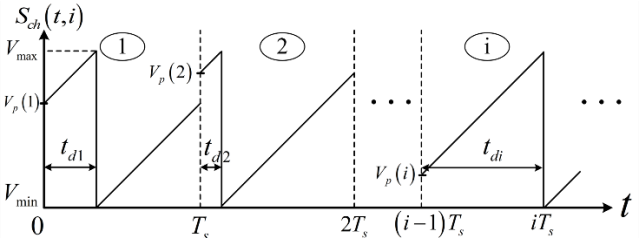

Fig. 4. Example of cyclic-shift chirp symbols.

$$y=\begin{cases} mx+c_1, & x_0 \le x < x_1, \\ mx+c_2, & x_1 \le x \le x_{\max} \end{cases} \tag{4}$$

where m is the slope of the linear line, x_1 is the intersection points on the x-axis, c_1 and c_2 are the intersection points on the y-axis of two parallel lines L_1 and L_2, respectively.

As the mathematical model for the cyclic-shift chirp symbol illustrated in Fig. 3 and an example of the cyclic-shift chirp symbols shown in Fig. 4, the cyclic-shift chirp symbol is represented by two intervals of a sawtooth signal. The y-axis represents the amplitude (or voltage level) of the symbol and the x-axis represents time. The mathematical expression is given by

$$S_{\mathrm{ch}}(t,i)= \begin{cases} \dfrac{V_{\max}-V_{\min}}{T_{\mathrm{s}}}\left(t-(i-1)T_{\mathrm{s}}\right)+V_{\mathrm{p}}(i), & (i-1)T_{\mathrm{s}} \le t \le (i-1)T_{\mathrm{s}}+t_{\mathrm{d}i}, \\ \dfrac{V_{\max}-V_{\min}}{T_{\mathrm{s}}}\left(t-iT_{\mathrm{s}}\right)+V_{\mathrm{p}}(i), & (i-1)T_{\mathrm{s}}+t_{\mathrm{d}i} \le t \le T_{\mathrm{s}} \end{cases} \tag{5}$$

where $V_{\mathrm{p}}(i)$ is the initial voltage level (corresponding to the initial phase) of the i^{th} symbol, $V_{\max}$ and $V_{\min}$ are the maximum and minimum amplitude, T_{s} is the period of a cyclic-shift chirp symbol, and $t_{\mathrm{d}i}$ denotes the duration of the first interval of the sawtooth signal corresponding to the i^{th} chirp symbol. The duty cycle of the chirp symbol is defined by

$$Duty\ cycle=\frac{t_{\mathrm{d}i}}{T_{\mathrm{s}}}=\frac{1}{T_{\mathrm{s}}}\left(t_{\mathrm{V}_{\max}}-t_{\mathrm{V_p(i)}}\right) \tag{6}$$

where $t_{\mathrm{V}_{\max}}$ and $t_{\mathrm{V_p(i)}}$ are time at the position of maximum amplitude and time at the beginning position of the i^{th} symbol, respectively.

3. Encoding and Decoding of the Cyclic-Shift Chirp Symbol

The generation of a chirp signal is done by using a voltage control oscillator (VCO) that takes a chirp symbol as its input. The chirp symbol is recovered at the receiver by using a FM demodulator. Due to lack of past research on encoding and decoding techniques for cyclic-shift chirp modulation, thus, this article proposes new encoding and decoding techniques for cyclic-shift chirp modulation and will be discussed in the following sections.

3.1 The Proposed Encoding Technique of the Cyclic-Shift Chirp Symbol

The generation of cyclic-shift chirp symbols is a crucial part of cyclic-shift chirp modulation. The generation can be done using either software or hardware. However, practical hardware techniques are lack in research study. Therefore, this paper presents a hardware technique for generating cyclic-shift chirp symbols, which consists of two parts.

1) Coding phase signal generating

The first part of the hardware technique for generating cyclic-shift chirp symbols involves generating a coding phase signal. The process as illustrated in Fig. 5 involves subtracting the analog level (A) related to the data bits from Vmax (M), comparing the output with a sawtooth carrier signal (B), and obtaining the PWM signal (C). The analog level is then combined with the sawtooth signal (D), modulated with the PWM signal, resulting in the coding phase signal (E).

The initial phase of the sawtooth signal is directly related to the data-bit symbol. Example waveforms ((A) to (E) and (M)) are shown in Fig. 6.

2) Reference phase signal generating

The reference phase signal is generated by a similar process where the block diagram is depicted in Fig. 7.

The signals at each stage of the block diagram are shown in Fig. 8.

The signal (F), obtained by subtracting the analog level (A) from the maximum level of the cyclic-shift chirp symbol (M), is multiplied by the inverse PWM signal ($\overline{C}$). The resulting signal (H) is then compared with the signal (G), which is the product of the carrier sawtooth signal (B) and inverse PWM. Thus, the output is the reference phase signal (I).

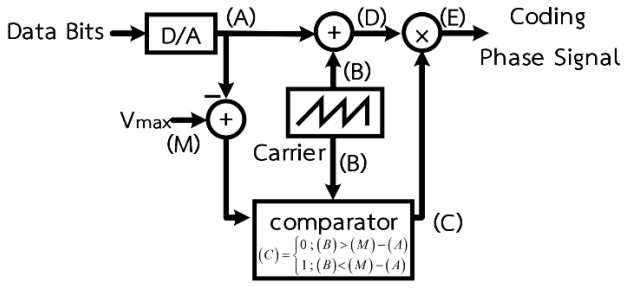

Fig. 5. Block diagram for generation of the coding phase signal.

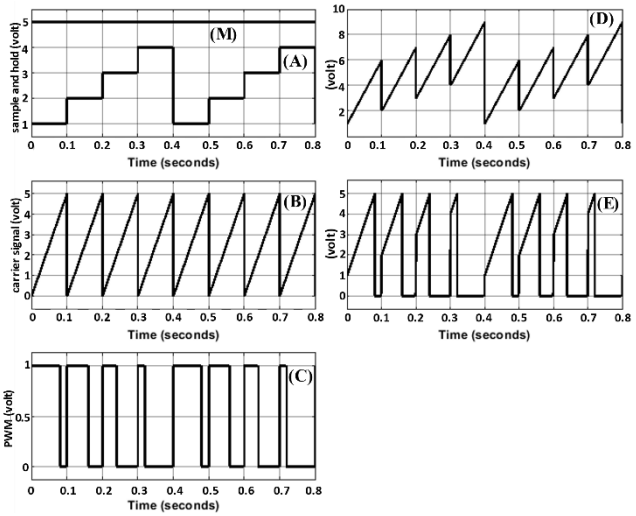

Fig. 6. Example waveforms of the block diagram for generation of the coding phase signal.

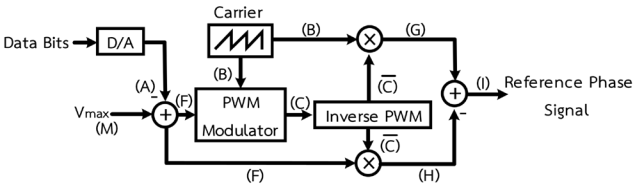

Fig. 7. Block diagram for generation of the reference phase signal.

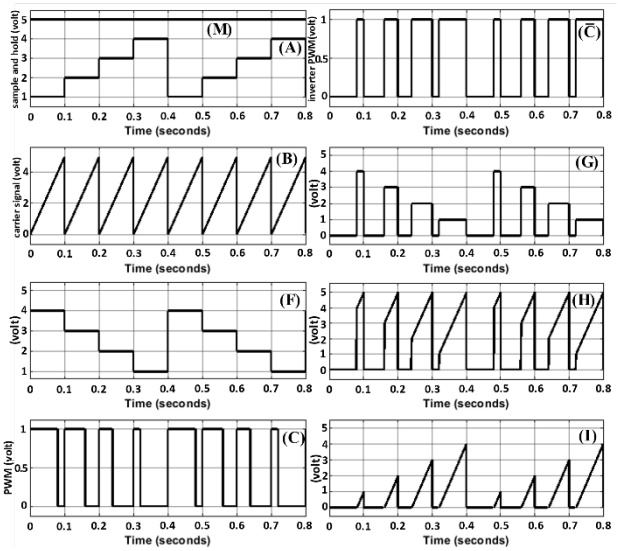

Fig. 8. Example waveforms of the block diagram for generation of the reference phase signal.

Combining the output signals of both parts forms the complete cyclic-shift chirp symbol. The combined block diagram for generation of the cyclic-shift chirp symbol is shown in Fig. 9, and the example signals (A), (E), (I), and (J) are illustrated in Fig. 10.

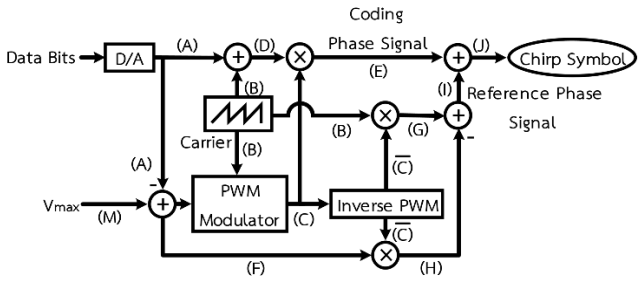

Fig. 9. Complete block diagram for generation of the cyclic-shift chirp symbol.

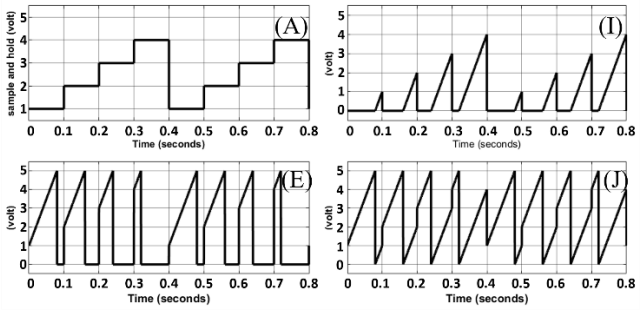

Fig. 10. Example waveforms of a block diagram for generation of the cyclic-shift chirp symbol.

The initial phase of each symbol is proportional to the data bit, while the second part of each bit time is the reference phase signal. The beginning and ending phases of each symbol are identical, which is a characteristic of a cyclic-shift chirp signal.

3.2 The Proposed Coherent Decoding Techniques: Addition and Subtraction Operations

The decoding technique for chirp symbols can be divided into two categories: coherent and non-coherent. The coherent decoding method requires synchronization in the demodulation process. In general, a preamble used for transmission detection, frame synchronization and frequency synchronization, is transmitted at the beginning of each packet. The traditional coherent decoding technique involves multiplying the chirp symbol and the negative ramp signal to decode the data bits [12]. However, this method has non-constant amplitude in the decoding signal, which results in ambiguity in determining the reference signal required for decoding. Therefore, an additional operation is needed to achieve a constant amplitude of the decoding signal. Example signals of this decoding method are shown in Fig. 11, where the top (A) and middle (B) traces are the chirp and negative ramp signals, respectively. The product output (C) (shown in the bottom trace) is a shape-like PWM and PAM signal whose amplitude of the positive and negative pulses is not constant.

To solve the issue of non-constant amplitude in traditional coherent decoding method, two new decoding techniques are proposed. The two new techniques are based on addition and subtraction operations and use positive and

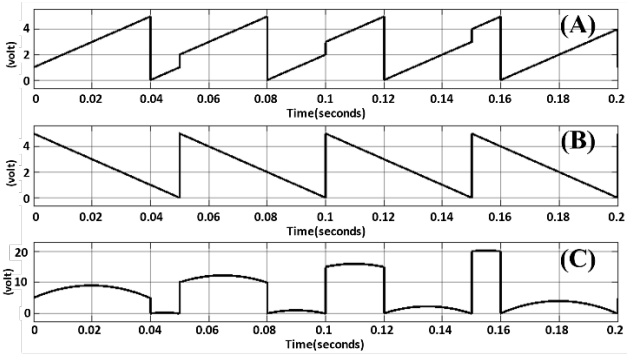

Fig. 11. Example waveforms of the coherent decoding technique based on multiplication operation [12].

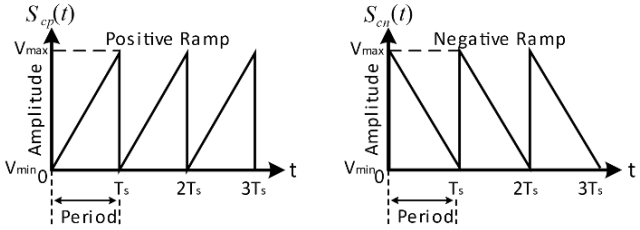

Fig. 12. Reference signals: (a) positive ramp, (b) negative ramp.

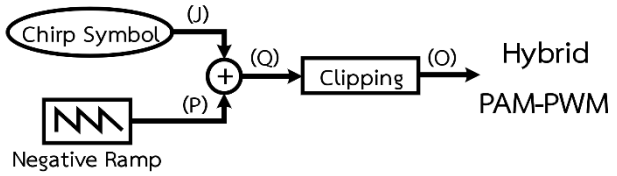

Fig. 13. Block diagram of coherent decoding based on addition operation technique.

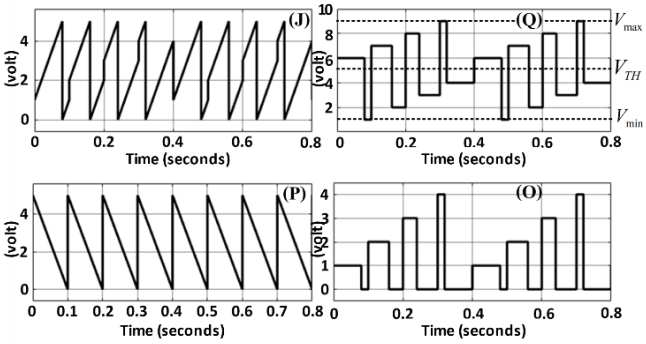

Fig. 14. Relationship among signals obtained from the block diagram of the coherent decoding based on addition operation technique.

negative ramp signals as necessary carrier signals (shown in Fig. 12).

The mathematical expressions for the i^{th} period of the positive ramp ($S_{\text{cp}}(t)$) and negative ramp signals ($S_{\text{cn}}(t)$), can be respectively defined by

$$S_{\text{cp}}\left(t-(i-1)T_{\text{s}}\right)= \frac{V_{\max}-V_{\min}}{T_{\text{s}}}\left(t-iT_{\text{s}}\right)+\left(V_{\max}-V_{\min}\right);(i-1)T_{\text{s}}\le t\le iT_{\text{s}}, \tag{7}$$

$$S_{\mathrm{cn}}\left(t-(i-1)T_{\mathrm{s}}\right)= -\frac{V_{\max}-V_{\min}}{T_{\mathrm{s}}}\left(t-iT_{\mathrm{s}}\right);(i-1)T_{\mathrm{s}}\le t\le iT_{\mathrm{s}}. \quad (8)$$

1) The coherent decoding based on addition operation technique

The block diagram of the technique based on addition operation is shown in Fig. 13, with the signals at each stage depicted in Fig. 14.

The technique begins by adding the received chirp symbol $S_{\mathrm{ch}}(t-(i-1)T_{\mathrm{s}})$ to the negative ramp signal $S_{\mathrm{cn}}(t-(i-1)T_{\mathrm{s}})$. Thus, the obtained signal (Q) is expressed as follows:

$$S_{\mathrm{ch}}\left(t-(i-1)T_{\mathrm{s}}\right)+S_{\mathrm{cn}}\left(t-(i-1)T_{\mathrm{s}}\right)= \begin{cases} V_{\max}-V_{\min}+V_{\mathrm{p}}(i) \\ \quad ;(i-1)T_{\mathrm{s}}\le t\le (i-1)T_{\mathrm{s}}+t_{\mathrm{d}i} \\ V_{\mathrm{p}}(i) \\ \quad ;(i-1)T_{\mathrm{s}}+t_{\mathrm{d}i}\le t\le iT_{\mathrm{s}}. \end{cases} \quad (9)$$

According to (9), during the encoding period ($t_{\mathrm{d}i}$) or the first interval, the output is proportional to $V_{\max}-V_{\min}+V_{\mathrm{p}}(i)$, whereas the output during the second interval ($T_{\mathrm{s}}-t_{\mathrm{d}i}$) is proportional to $V_{\mathrm{p}}(i)$. When this signal is clipped [21] using the reference voltage ($V_{\mathrm{TH}}=(V_{\max}-V_{\min})/2$), the decoded signal (O) is given by

$$S_{\mathrm{clip}}\left(t-(i-1)T_{\mathrm{s}}\right)= \begin{cases} V_{\mathrm{p}}(i), & (i-1)T_{\mathrm{s}}\le t\le (i-1)T_{\mathrm{s}}+t_{\mathrm{d}i}, \\ 0, & (i-1)T_{\mathrm{s}}+t_{\mathrm{d}i}\le t\le iT_{\mathrm{s}}. \end{cases} \quad (10)$$

The expression shown by (10) indicates that the positive-pulse amplitude is proportional to the information signal $V_{\mathrm{p}}(i)$, whereas the negative-pulse amplitude is always zero. Therefore, the decoded signal can be considered as a PAM signal whose duty cycle is in accordance with (6). The difference is that the signal expressed by (5) is a sawtooth signal whereas the signal shown by (10) is a square-wave signal. In addition, width of the positive pulse is proportional to $V_{\mathrm{p}}(i)$, it thus can be considered as a PWM signal as well. Hence, the decoded signal of the proposed decoding based on addition technique is a hybrid PAM-PWM waveform.

2) The coherent decoding based on subtraction operation technique

The subtraction operation technique is similar to the technique of addition operation as the block diagram of decoding process shown in Fig. 15. Figure 16 demonstrates the example of signals at each state of the decoding process.

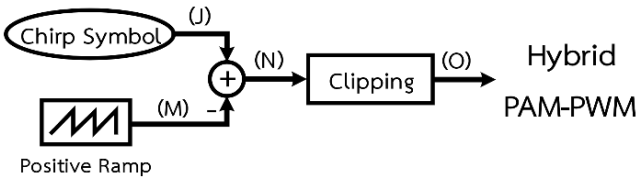

Fig. 15. Block diagram for coherent decoding based on subtraction operation technique.

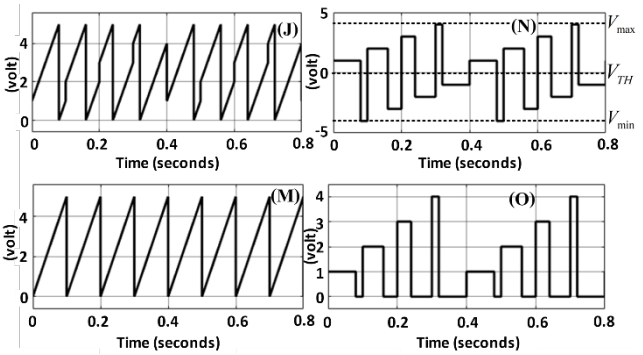

Fig. 16. Relationship among signals obtained from the block diagram of the coherent decoding based on subtraction operation technique.

Firstly, the received chirp symbol $S_{\mathrm{ch}}(t-(i-1)T_{\mathrm{s}})$ is subtracted from the positive ramp signal $S_{\mathrm{cp}}(t-(i-1)T_{\mathrm{s}})$, and the output signal (N) is as follows:

$$S_{\mathrm{ch}}\left(t-(i-1)T_{\mathrm{s}}\right)-S_{\mathrm{cp}}\left(t-(i-1)T_{\mathrm{s}}\right)= \begin{cases} V_{\mathrm{p}}(i), & (i-1)T_{\mathrm{s}}\le t\le (i-1)T_{\mathrm{s}}+t_{\mathrm{d}i}, \\ V_{\mathrm{p}}(i)-V_{\max}+V_{\min}, & \\ \quad (i-1)T_{\mathrm{s}}+t_{\mathrm{d}i}\le t\le iT_{\mathrm{s}}. & \end{cases} \quad (11)$$

Note that during the first interval, the amplitude is proportional to the information signal $V_{\mathrm{p}}(i)$, whereas the amplitude during the second interval is proportional to $V_{\mathrm{p}}(i)-V_{\max}+V_{\min}$. After rectifying by the 0 V reference signal ($V_{\mathrm{TH}}=0$), the decoded signal (O) which is a hybrid PAM-PWM signal is obtained.

In summary, the decoded signal obtained from two proposed coherent decoding techniques based on addition and subtraction operations is shape-like hybrid PAM-PWM signal. As the relationship between cyclic-shift chirp symbol and pulse modulation discussed in Sec. 2.2, the decoded signal provides flexibility in recovering the information data bits which can be retrieved from either amplitude of PAM or width of PWM. Additionally, since the amplitude of the decoded signal is constant, the nonlinear problem caused by the multiplication operation [12] is solved.

3.3 Encoding Cyclic-Shift Chirp Symbol for *n* Data Bits

In this subsection, the procedure to design the encoding cyclic-shift chirp symbol for n data bits using the proposed encoding technique mentioned in Sec. 3.1 is given. The procedure comprises of the following steps:

1. Define the minimum and maximum frequency of the chirp signal [$f_{\min}, f_{\max}$].

2. Define the minimum and maximum voltage of the sawtooth signal corresponding to the minimum and maximum frequency [$V_{\min}, V_{\max}$].

3. Define all possible voltage levels $V_{\mathrm{p}}(i)$ to obtain 2^n phases, where the difference voltage of each level is $\Delta V=(V_{\max}-V_{\min})/(2^N+1)$, which can be determined as follows:

$$V_{\mathrm{p}}(i) = V_{\min} + i(\Delta V), \qquad i = 1,2,3,...,2^n. \tag{12}$$

4. Design an n-bit D/A to provide an analog output corresponding to the 2^n voltage levels of $V_{\mathrm{p}}(i)$ in step 3.

5. Define the period of the cyclic-shift chirp symbol or sawtooth signal, which relates to the bit rate transmission D (bps) and baud rate B (symbols/s) as follows:

$$D = B\log_2 2^n = nB \tag{13}$$

and

$$B = \frac{1}{T_{\mathrm{s}}}. \tag{14}$$

Therefore,

$$T_{\mathrm{s}} = \frac{n}{D}. \tag{15}$$

From the encoding procedure stated above, an example for encoding 2 bits/symbol of cyclic-shift chirp is given as follows:

1. $[f_{\min}, f_{\max}] = [25\text{ kHz}, 35\text{ kHz}]$

2. Let k_{f} of VCO be 2 kHz/V and $[V_{\min}, V_{\max}]$ are [0, 5 V].

3. $V_{\mathrm{p}}(i) = 0 + i\left(\dfrac{5-0}{2^2+1}\right) = i(1)\ ;\ i = 1,2,3,4$

4. $i = D_1 \times 2^1 + D_0 \times 2^0 + 1$ where D_1, D_0 are most and least significant bit, respectively and the voltage of initial phase is $V_{\mathrm{p}}(i) = i$, which corresponding to the initial phase is $i(2\pi/5)$ radians.

5. $D = 9600$ bps, then $T_{\mathrm{s}} = n/D = 2/9600$ s and $B = 1/T_{\mathrm{s}} = 4800$ symbols/s.

3.4 Spectral and Bandwidth Analysis

This subsection describes the mathematical analysis of the bandwidth of a chirp signal. The standard method of calculating the bandwidth of a chirp signal is given by (3) but a different approach is also presented in this subsection. The new approach involves considering the chirp signal as a frequency modulated (FM) signal, where the information signal is represented by a chirp symbol. The chirp symbol has positive and negative slopes (s and $-s$ respectively) to encode data bits "1" and "0". Figure 17 shows examples of chirp symbols for consecutive data bits "0" (upper), "1" (middle), and alternating "1" and "0" (bottom). These chirp symbols are shaped like negative slope sawtooth signals, positive slope sawtooth signals, and triangular wave signals, respectively.

To calculate the effective bandwidth, a mathematical analysis will be derived based on the positive-slope sawtooth signal. As per (7), for i equal to 1, one period of the positive-slope sawtooth signal can be expressed as follows:

$$S_{\mathrm{cp}}(t) = \frac{V_{\max} - V_{\min}}{T_{\mathrm{s}}} t, \qquad 0 \le t \le T_{\mathrm{s}}. \tag{16}$$

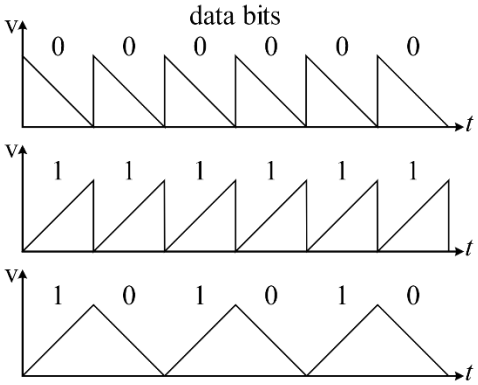

Fig. 17. Example of chirp symbols used in the analysis.

The output frequency when the positive-slope sawtooth signal is fed to a VCO with a frequency sensitivity of k_{f} is expressed as follows:

$$\begin{aligned} f_{\mathrm{vco}}(t) &= k_{\mathrm{f}} S_{\mathrm{cp}}(t) + f_{\min} = k_{\mathrm{f}}\left[\frac{V_{\max} - V_{\min}}{T_{\mathrm{s}}} t\right] + f_{\min} \\ &= \frac{(f_{\max} - f_{\min})}{T_{\mathrm{s}}} t + f_{\min} = \frac{\Delta}{T_{\mathrm{s}}} t + f_{\min} \end{aligned} \tag{17}$$

where Δ is $(f_{\max} - f_{\min})$ and the output of the VCO is the FM signal, which can be written as

$$\begin{aligned} \phi_{\mathrm{FM}}(t) &= A_{\mathrm{c}}\, \mathrm{e}^{\mathrm{j}2\pi\left\{f_{\mathrm{c}} t + k_{\mathrm{f}} \int S_{\mathrm{cp}}(t)\mathrm{d}t\right\}} = A_{\mathrm{c}}\, \mathrm{e}^{\mathrm{j}2\pi\left\{f_{\mathrm{c}} t + \int \frac{\Delta}{T_{\mathrm{s}}} t \mathrm{d}t\right\}} = \\ &A_{\mathrm{c}}\, \mathrm{e}^{\mathrm{j}2\pi\left\{f_{\mathrm{c}} t + \frac{\Delta}{2T_{\mathrm{s}}} t^2\right\}} = F_0 + \sum_{n=-\infty}^{\infty} F_n\, \mathrm{e}^{\mathrm{j}n2\pi f_0 t}. \end{aligned} \tag{18}$$

In (18), A_{c} represents the amplitude of the FM signal (volt), f_{c} is the carrier frequency (Hz), k_{f} is the sensitivity or gain of the VCO (Hz/volt) , and f_0 is the fundamental frequency of the chirp symbol (Hz), which is inversely proportional to the duration T_{s}. The exponential Fourier series coefficient F_n can be determined by

$$F_n = \frac{1}{T_{\mathrm{s}}} \int_0^{T_{\mathrm{s}}} \phi_{\mathrm{FM}}(t)\, \mathrm{e}^{-\mathrm{j}n2\pi f_0 t}\, \mathrm{d}t \tag{19}$$

where T_{s} is the period of the chirp symbols, $\phi_{\mathrm{FM}}(t)$ is the frequency modulated signal, f_0 is the fundamental frequency (Hz). When substituting (18) into (19), the following expression is obtained:

$$F_n = \frac{1}{T_{\mathrm{s}}} \int_0^{T_{\mathrm{s}}} A_{\mathrm{c}}\, \mathrm{e}^{\mathrm{j}2\pi\left\{(f_{\mathrm{c}} - nf_0)t + \frac{\Delta}{2T_{\mathrm{s}}} t^2\right\}}\, \mathrm{d}t. \tag{20}$$

According to (20), the Fresnel integrated form [22] is obtained where

$$\alpha = 2\left(\sqrt{\frac{\Delta}{2T_{\mathrm{s}}}} t + (f_{\mathrm{c}} - nf_0)\left(\sqrt{\frac{T_{\mathrm{s}}}{2\Delta}}\right)\right) \tag{21}$$

and

$$Z(u)=C(u)+\mathrm{j}S(u)=\int_0^u \mathrm{e}^{\mathrm{j}\pi\alpha^2/2}\,\mathrm{d}\alpha; \tag{22}$$

then (20) is rewritten as follows:

$$\begin{aligned}F_n &= A_\mathrm{c}\sqrt{\frac{1}{T_\mathrm{s}2\Delta}}\,\mathrm{e}^{-\mathrm{j}2\pi(f_\mathrm{c}-nf_0)^2\left(\frac{T_\mathrm{s}}{2\Delta}\right)}\left[\int_0^{u_2}\mathrm{e}^{\mathrm{j}\pi\frac{\alpha^2}{2}}\,\mathrm{d}\alpha-\int_0^{u_1}\mathrm{e}^{\mathrm{j}\pi\frac{\alpha^2}{2}}\,\mathrm{d}\alpha\right]\\ &= A_\mathrm{c}\sqrt{\frac{1}{T_\mathrm{s}2\Delta}}\,\mathrm{e}^{-\mathrm{j}2\pi(f_\mathrm{c}-nf_0)^2\left(\frac{T_\mathrm{s}}{2\Delta}\right)}\left[\begin{array}{l}\left\{\int_0^{u_2}\cos\left(\pi\frac{\alpha^2}{2}\right)\mathrm{d}\alpha+\int_0^{u_2}\mathrm{j}\sin\left(\pi\frac{\alpha^2}{2}\right)\mathrm{d}\alpha\right\}\\ -\left\{\int_0^{u_1}\cos\left(\pi\frac{\alpha^2}{2}\right)\mathrm{d}\alpha+\int_0^{u_1}\mathrm{j}\sin\left(\pi\frac{\alpha^2}{2}\right)\mathrm{d}\alpha\right\}\end{array}\right]\\ &= A_\mathrm{c}\sqrt{\frac{1}{T_\mathrm{s}2\Delta}}\,\mathrm{e}^{-\mathrm{j}2\pi(f_\mathrm{c}-nf_0)^2\left(\frac{T_\mathrm{s}}{2\Delta}\right)}\left[Z(u_2)-Z(u_1)\right].\end{aligned} \tag{23}$$

By defining u_1 and u_2 as in (24) and (25):

$$u_1=-\sqrt{\frac{\Delta T_s}{2}}+2\left(f_\mathrm{c}-nf_0\right)\left(\sqrt{\frac{T_\mathrm{s}}{2\Delta}}\right), \tag{24}$$

$$u_2=\sqrt{\frac{\Delta T_\mathrm{s}}{2}}+2\left(f_\mathrm{c}-nf_0\right)\left(\sqrt{\frac{T_\mathrm{s}}{2\Delta}}\right), \tag{25}$$

and using the relation between the exponential Fourier series coefficient and trigonometry Fourier series coefficient: $F_n=\frac{a_n}{2}+\frac{b_n}{2\mathrm{j}}$, a_n and b_n are expressed by

$$a_n = A_\mathrm{c}\sqrt{\frac{2}{T_\mathrm{s}\Delta}}\left(\begin{array}{l}\cos\left(\pi\left(f_\mathrm{c}-nf_0\right)^2\left(\frac{T_\mathrm{s}}{\Delta}\right)\right)\sum_{k=0}^{\infty}\frac{(-1)^k\left(\frac{1}{2}\pi\right)^{2k}\left(u_2^{\,4k+1}-u_1^{\,4k+1}\right)}{(2k)!(4k+1)}\\ +\sin\left(\pi\left(f_\mathrm{c}-nf_0\right)^2\left(\frac{T_\mathrm{s}}{\Delta}\right)\right)\sum_{k=0}^{\infty}\frac{(-1)^k\left(\frac{1}{2}\pi\right)^{2k+1}\left(u_2^{\,4k+3}-u_1^{\,4k+3}\right)}{(2k+1)!(4k+3)}\end{array}\right),$$

$$b_n = -A_\mathrm{c}\sqrt{\frac{2}{T_\mathrm{s}\Delta}}\left(\begin{array}{l}\cos\left(\pi\left(f_\mathrm{c}-nf_0\right)^2\left(\frac{T_\mathrm{s}}{\Delta}\right)\right)\sum_{k=0}^{\infty}\frac{(-1)^k\left(\frac{1}{2}\pi\right)^{2k+1}\left(u_2^{\,4k+3}-u_1^{\,4k+3}\right)}{(2k+1)!(4k+3)}\\ -\sin\left(\pi\left(f_\mathrm{c}-nf_0\right)^2\left(\frac{T_\mathrm{s}}{\Delta}\right)\right)\sum_{k=0}^{\infty}\frac{(-1)^k\left(\frac{1}{2}\pi\right)^{2k}\left(u_2^{\,4k+1}-u_1^{\,4k+1}\right)}{(2k)!(4k+1)}\end{array}\right). \tag{26}$$

By using the trigonometry Fourier series coefficients, the plots of one-side magnitude spectra; determined by $c_n=\sqrt{a_n^2+b_n^2}$; for frequency deviation $\Delta_1=7$ kHz and $\Delta_2=10$ kHz where the fundamental frequency of chirp symbol f_0 is 10 Hz and carrier frequency f_c is 30 kHz are depicted in Fig. 18.

The obtained –3dB bandwidths, defined by $f_{3\mathrm{dBH}}-f_{3\mathrm{dBL}}$, are 7 kHz and 10 kHz, respectively, which are in accordance with the setting parameters.

Typically, $f_{3\mathrm{dBH}}=f_{\min}+\mu T_\mathrm{S}$ and $f_{3\mathrm{dBL}}=f_{\min}+\mu(0)$ for $0\le t\le T_\mathrm{s}$, therefore, the bandwidth of the chirp signal can be

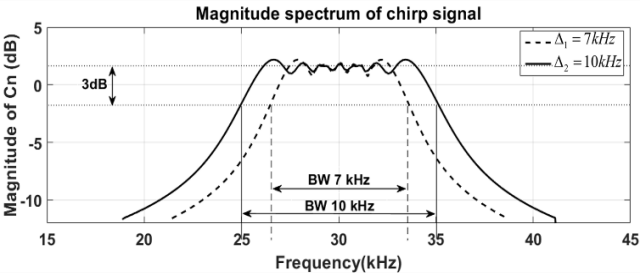

Fig. 18. Example magnitude spectrum of chirp signal plotted by using the foraminal trigonometry Fourier series coefficients.

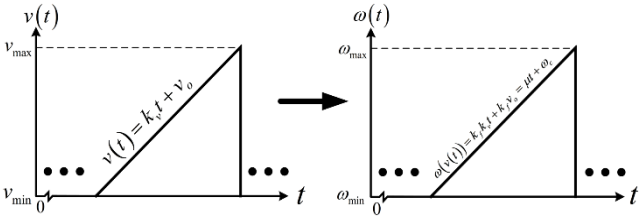

Fig. 19. Graphical relation between input signal and output frequency of the VCO.

calculated by

$$\begin{aligned}BW &= f(T_\mathrm{s})-f(0)\\ &=\left(f_{\min}+\mu(T_\mathrm{s})\right)-\left(f_{\min}+\mu(0)\right)=\mu T_\mathrm{s}.\end{aligned} \tag{27}$$

From Fig. 18, it is found that $f_{\min}=26.5$ kHz and $\mu_1=1.05\times10^5$ Hz/s for $\Delta_1=7$ kHz, $f_{\min}=25$ kHz and $\mu_2=1.5\times10^5$ Hz/s for $\Delta_2=10$ kHz. For $T_\mathrm{s}=1/f_0$, the calculated bandwidths for both cases using (27) are also confirmed to be 7 kHz and 10 kHz.

In this paper, an alternative method for approximating the bandwidth of the chirp signal is proposed. The relationship between the input voltage and output frequency of the VCO is considered, as the chirp signal is generated by feeding the chirp symbol as an input to the VCO. The relationship is graphically represented in Fig. 19, with the mathematical expression provided as

$$\omega\left(v(t)\right)=k_\mathrm{f}k_\mathrm{v}t+k_\mathrm{f}v_\mathrm{o}=\mu t+\omega_\mathrm{c} \tag{28}$$

where v_o voltage level at free running state of the VCO.

As seen in (28), the chirp rate μ is $k_\mathrm{v}k_\mathrm{f}=(\Delta v/\Delta t)\cdot(\Delta\omega/\Delta v)=\Delta\omega/\Delta t$ (rad/s^2) where Δv, $\Delta\omega$ and Δt are the change of voltage, frequency and time, respectively. Hence, by comparing to (27), bandwidth of the chirp signal can be approximated by

$$BW\approx k_\mathrm{f}k_\mathrm{v}T_\mathrm{s}. \tag{29}$$

3.5 Error Performance Analysis of 4-Cyclic Shift Chirp Signal

In this section, an error analyses of the 4-cyclic shift chirp signal are conducted, similar to [23], [24]. They consider a set of 4-cyclic shift chirp symbols, where each sym-

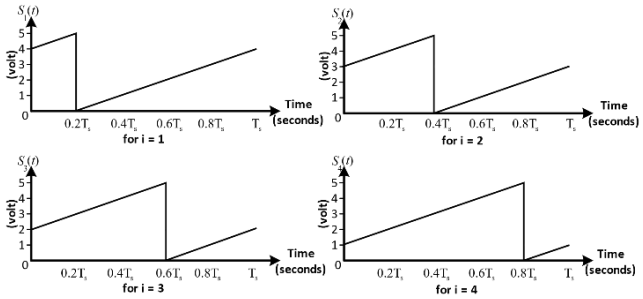

Fig. 20. Graphical representation of 4-cyclic shift chirp symbols.

bol (i = 1, 2, 3, 4) can be expressed mathematically as follows:

$$s_i(t)=\begin{cases}\mu\left(t+T_s\left(1-\dfrac{i}{5}\right)\right), & 0<t<i\dfrac{T_s}{5},\\ \mu\left(t-i\dfrac{T_s}{5}\right), & i\dfrac{T_s}{5}<t<T_s\end{cases} \tag{30}$$

and graphical representation of four symbols is shown in Fig. 20.

According to Fig. 20, the normalized correlation of the 4-cyclic shift chirp symbols ($\rho(s_i,s_j)$) is described as follows:

$$\rho\left(s_i,s_j\right)=\frac{1}{E_s}\int_0^{T_s}s_i(t)s_j(t)\,\mathrm{d}t \tag{31}$$

where E_s is the energy of the cyclic-shift chirp symbol. When the 4-cyclic shift chirp symbols are combined and correlated, the total of six correlations are produced, denoted as $\rho(s_i,s_j)$, $i\neq j$ for i, j = 1,2,3,4. The results are depicted in Fig. 21.

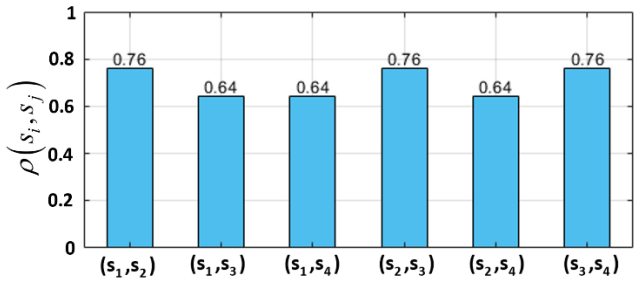

Fig. 21. Normalized values of six correlations of 4-cyclic shift chirp symbols.

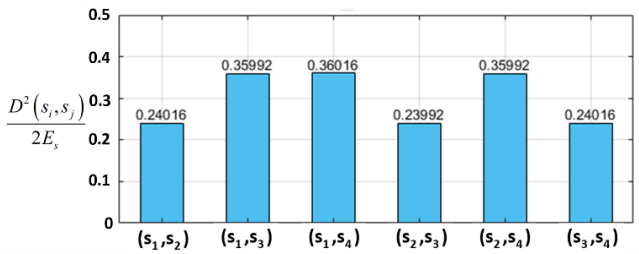

Fig. 22. Six normalized squared Euclidean distances of 4-cyclic shift chirp symbols.

Next, the correlation value is used to calculate the squared Euclidean distance $D^2(s_i,s_j)$ as follows:

$$D^2\left(s_i,s_j\right)=2E_s\left(1-\rho\left(s_i,s_j\right)\right). \tag{32}$$

The squared Euclidean distance is normalized by $2E_s$; the results are shown in Fig. 22.

According to Fig. 22, the lowest value is taken to calculate the maximum probability as given by

$$P_e\simeq Q\left(\sqrt{\frac{D_{\min}^2}{2N_0}}\right)\simeq Q\left(\sqrt{\frac{\left(0.23992\times 2E_s\right)}{2N_0}}\right). \tag{33}$$

For Rayleigh fading probability (P_{erf}), it is given by

$$P_{erf}=\frac{1}{\pi}\int_0^{\pi/2}\frac{\sin^2\theta}{\dfrac{E_s}{N_0}\left(1-\rho(i,j)\right)+\sin^2\theta}\,\mathrm{d}\theta \tag{34}$$

whose maximum value of P_{erf} is obtained when $\rho(s_1,s_2)$ = 0.76 [24], [25].

4. Simulation and Experiment Results

4.1 Simulation Results

In this section, the encoding and decoding of 4-cyclic shift chirp symbols, each representing two data bits, are simulated using MATLAB. The block diagram using for encoding and decoding the 4-cyclic shift chirp symbols based on the proposed techniques is depicted in Fig. 23.

The parameters in this simulation are: frequency of chirp symbol f_0 = 10 Hz, minimum frequency of chirp signal f_{min} = 25 kHz, maximum frequency of chirp signal f_{max} = 35 kHz, gain of VCO k_f = 2 kHz/volt, and k_v = 5 volt/ms. The results of the simulation results are shown in Fig. 24.

Figure 24(a) shows the analog level representing each two-bit pattern and Figure 24(b) depicts the corresponding 4-cyclic shift chirp symbol. It can be seen that the initial and

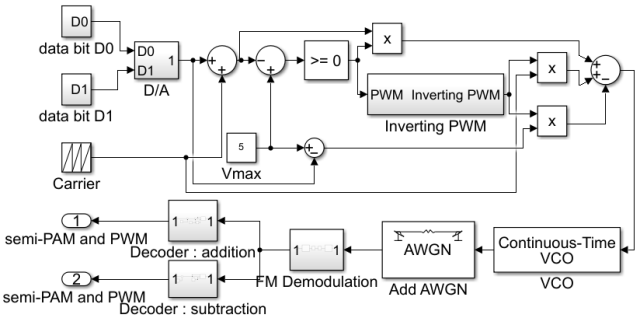

Fig. 23. Blocks diagram for encoding and decoding of 4-cyclic shift chirp signals based on the proposed techniques.

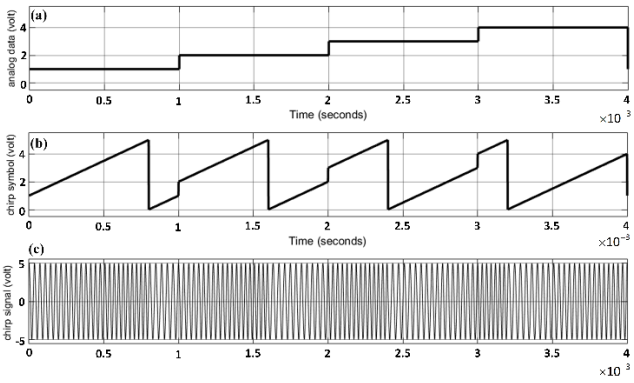

Fig. 24. Four cyclic-shift chirp symbols and signals: (a) analog data, (b) 4-cyclic shift chirp symbols, and (c) 4-cyclic shift chirp signal.

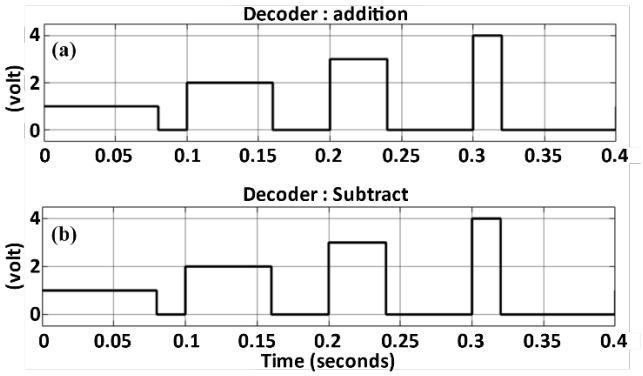

Fig. 25. Decoder outputs of 4-cyclic shift chirp based on the proposed algorithms (a) addition, (b) subtraction.

ending voltage levels of each symbol are equal, which is a characteristic of cyclic-shift chirp symbols. As seen in Fig. 24(c), the frequency of the chirp signal varies according to the magnitude of the cyclic-shift chirp symbols.

The decoding process takes place in the receiver, which consists of an FM demodulator and a cyclic-shift chirp decoder. The simulation results of the two proposed decoding techniques (addition and subtraction algorithms) are shown in Fig. 25.

It is observed that the decoded signals from both techniques are in the form of a hybrid pulse amplitude modulation (PAM)-pulse width modulation (PWM) waveform. Furthermore, the amplitude and width of the first interval of each period of the decoder output are related to the information, and the data can be retrieved from either the amplitude or width of the decoder output when compared to the cyclic-shift chirp symbol at the transmitting side (Fig. 24(b)).

In addition, when the chirp signal shown in Fig. 24(c) is passed through a spectrum analyzer, the bandwidth of the signal is shown in Fig. 26.

The –3dB bandwidth, as determined from the graph, is 10 kHz. To confirm the approximated bandwidth analysis presented in Sec. 3.4, the bandwidth calculated using (29) for $k_f = 2$ kHz/volt, $k_v = 5$ volt/ms, and $T_s = 1/f_0 = 1$ ms is 10 kHz. Thus, it is confirmed the proposed mathematical

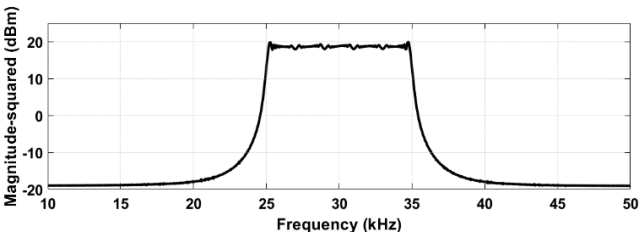

Fig. 26. Spectrum of chirp signal from simulation.

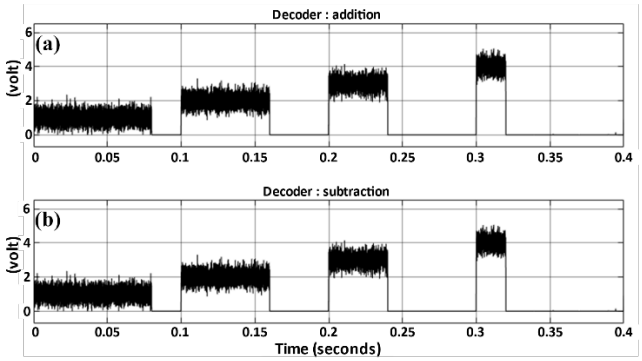

Fig. 27. Decoder outputs of 4-cyclic shift chirp based on the proposed algorithms for SNR = 5 dB: (a) addition, (b) subtraction.

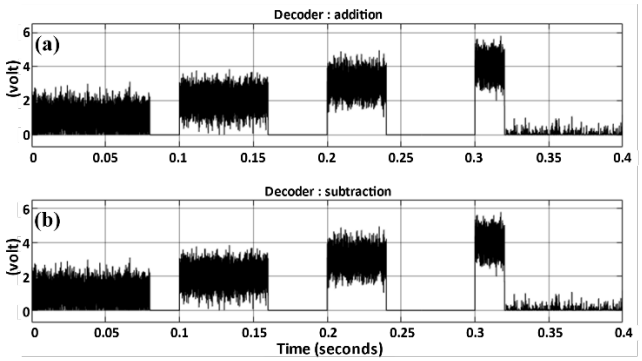

Fig. 28. Decoder outputs of 4-cyclic shift chirp based on the proposed algorithms for SNR = 10 dB: (a) addition, (b) subtraction.

analysis for bandwidth approximation of the cyclic-shift chirp signal agrees well with the simulation result.

In this study, the error probability performance of the 4-cyclic shift chirp data transmission is simulated under additive white Gaussian noise. Figures 27 and 28 illustrate the decoded signals using addition and subtraction algorithms for SNR values of 5 dB and 10 dB, respectively.

The error probability of the proposed technique for additive white Gaussian noise for analytical (calculated using (33)) and simulation in the range of 0–35 dB is depicted by the black bold line and triangle plot in Fig. 29.

The error probability for 2-ary chirp and 4-ary chirp over Rayleigh fading channel from [23] is shown by the dash-dotted line and dash line, respectively. The dotted line and star symbol represent the analytical (calculated using (34)) and simulation Rayleigh fading probability of the 4-cyclic shift chirp signal, respectively.

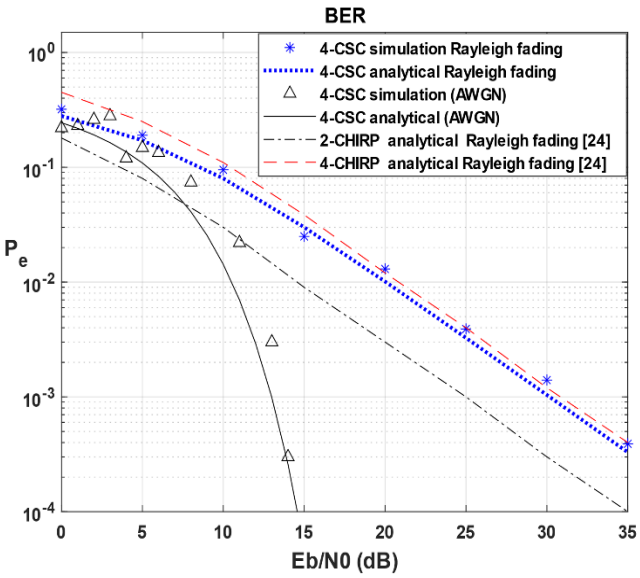

Fig. 29. Error probability performance.

4.2 Experiment Results

To confirm the process for generating encode and decode 4-cyclic shift chirp that it is proposed as Fig. 9, Fig. 13 and Fig. 15, the analog circuit is fabricated by the discrete devices which the multiplier circuit is constructed with IC operational transconductance amplifier (OTA) No.13700 and their input and output are modified with attenuating input and amplifying output signals in order to get ideal multiplier because of pure OTA has linear operation input about 100 mV while the pure output form OTA multiplier is amplified by non-inverting amplifier 15 of gain and IC XR2206 is used to be voltage controlled oscillator for generating chirp signal and all of circuits are shown in Fig. 30. Voltage supply +V and −V are +6 V and −6 V, respectively.

For experimental results from the real circuit, which is shown in Fig. 30, the 10 Hz frequency of ramp signal is provided, 5 V_{pp} amplitude and offset DC 2.5 V and R = 1 kΩ, R_f = 10 kΩ, R_x = 13 kΩ and R_y = 1 kΩ. All of experimental results are shown in Fig. 31 to Fig. 35.

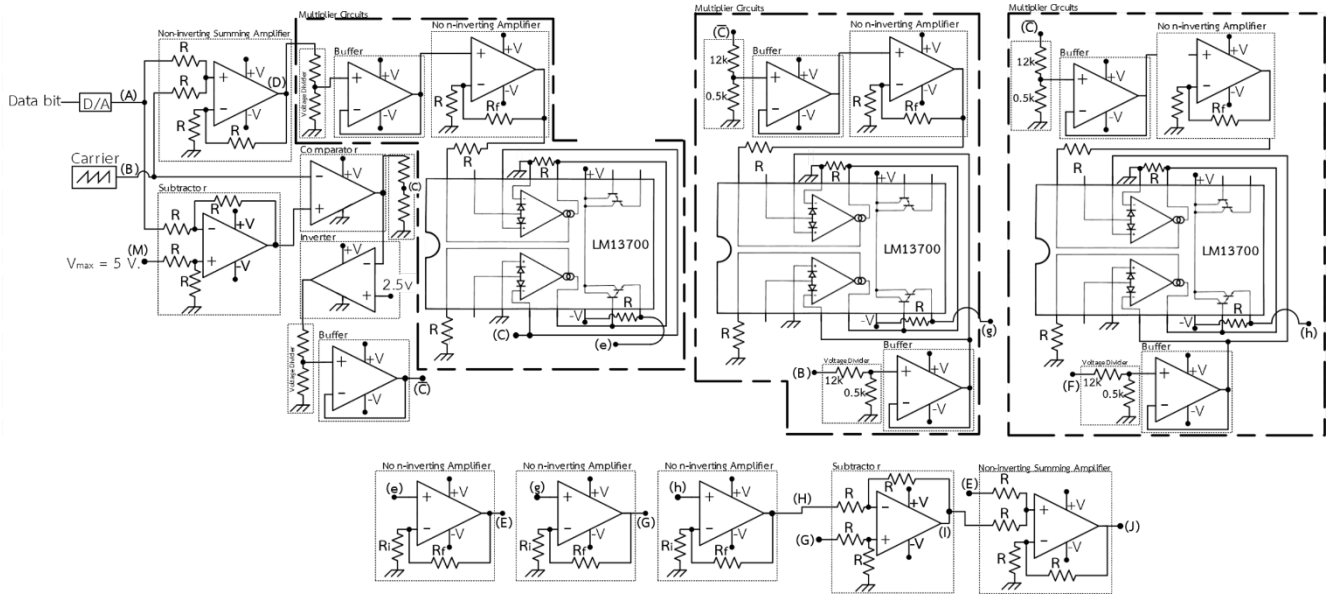

(a) The encoding circuits.

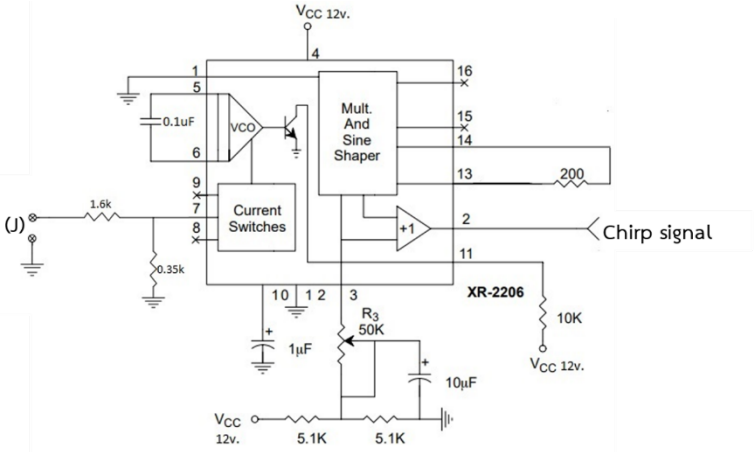

(b) The voltage control oscillator with XR2206.

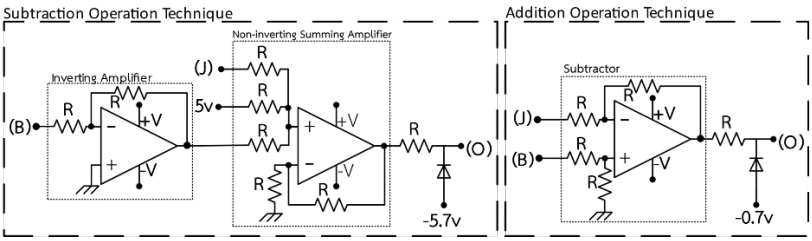

(c) The decoding circuits.

Fig. 30. The encoding and the decoding circuits based on the proposed techniques.

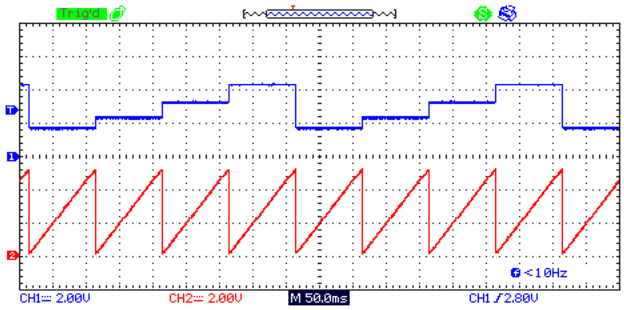

(a) The upper trace is analog data (A) and the bottom trace is positive ramp (B).

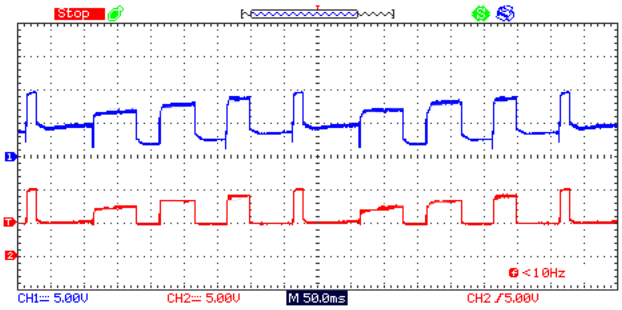

(b) The upper trace is output from summing amplifier for decoding addition operation technique (Q) and the bottom trace is a hybrid PAM-PWM from clipping operation (O).

Fig. 32. The coherent decoding experiment results based on addition operation technique.

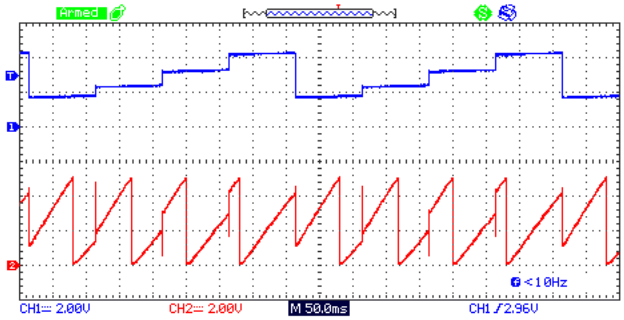

(b) The upper trace is analog data (A) and the bottom trace is 4-cyclic shift chirp symbols (J).

Fig. 31. The 4-cyclic shift chirp symbols experiment results.

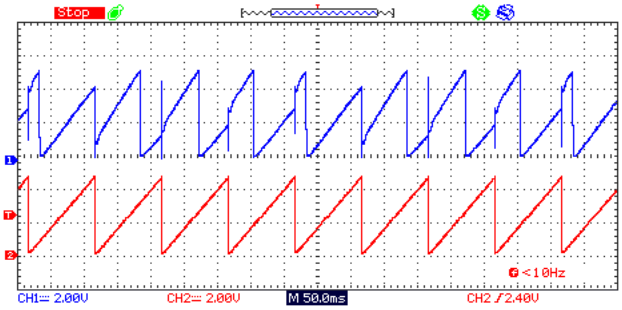

(a) The upper trace is 4-cyclic shift chirp symbols (J) and the bottom trace is positive ramp (M).

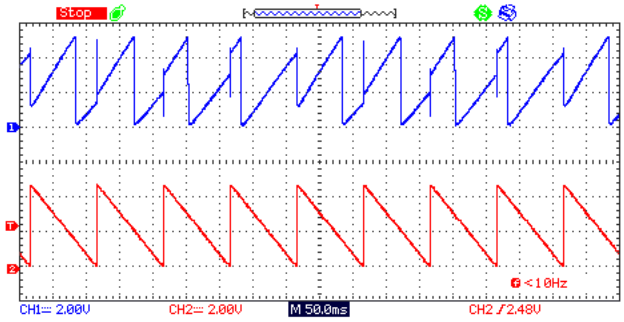

(a) The upper trace is 4-cyclic shift chirp symbols (J) and the bottom trace is negative ramp (P).

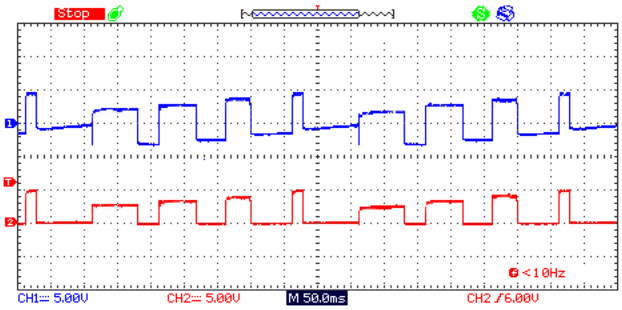

(b) The upper trace is output from differential amplifier for decoding subtraction operation technique (N) and the bottom trace is a hybrid PAM-PWM from clipping operation (O).

Fig. 33. The coherent decoding experiment results based on subtraction operation technique.

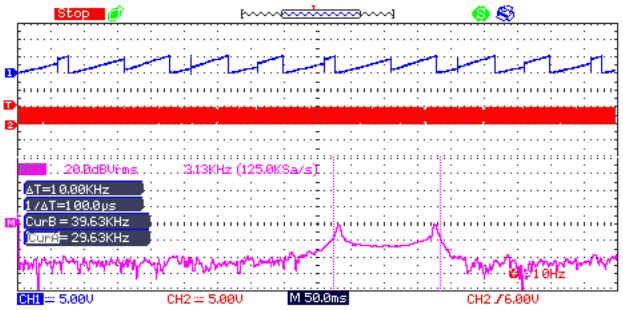

Fig. 34. Illustration of experiment results of 4-cyclic shift chirp symbols (J), chirp signal and spectrum of chirp signal. The upper trace is 4-cyclic shift chirp symbols, the middle trace is chirp signal and the bottom trace is spectrum of chirp signal.

5. Conclusions

This study proposes techniques and a mathematical analysis for encoding and decoding the 4-cyclic shift chirp signal. The proposed encoding method is simple to implement and is based on a mathematical model of the cyclic-shift chirp symbol. The proposed decoding technique employs two coherent methods, one based on addition and another on subtraction. The resulting decoded signal is a hybrid PAM-PWM waveform, providing flexibility in demodulating the information signal, which can be retrieved from either amplitude or width. Additionally, the decoded signal has constant amplitude, improving the accuracy of determining the reference signal compared to conventional techniques [12]. The relationship between cyclic-shift chirp modulation and pulse modulation (PAM, PWM, PPM) is discussed to understand how the information of the chirp symbol is represented in amplitude, width, or pulse position. The analytical frequency components of the cyclic-shift chirp signal are presented to determine its bandwidth, and a formula for approximating its bandwidth is obtained. The error performance of the 4-cyclic shift chirp signal under additive white Gaussian noise and fading noise is also analyzed. To validate the proposed techniques and mathematical analysis, the simulations and experiment of the 4-cyclic shift chirp signal were conducted using MATLAB and a real circuit, respectively. The results show that the proposed encoding and decoding methods effectively modulate and demodulate the 4-cyclic shift chirp signal, and the bandwidth determined from simulation and experiment matches that obtained using the proposed formula. The error probability performance of the 4-cyclic shift chirp signals under additive white Gaussian noise and fading noise is also demonstrated and is shown to have similar behavior to other techniques. Moreover, the experiment with real circuits show that the proposed technique can also work well in hardware.

Acknowledgments

This research was funded by the National Science, Research and Innovation Fund (NSRF), and King Mongkut's University of Technology North Bangkok with contract no. KMUTNB-FF-65-15.

References

[1] LATHI, B. P. *Modern Digital and Analog Communication System*. 3rd ed. New York (USA): Oxford University Press, 1998. Ch. 4, Amplitude (linear) modulation, p. 151–250. ISBN: 0-19-511009-9

[2] FOROUZAN, B. A. *Data Communications and Networking*. 4th ed. New York (USA): McGraw-Hill, 2007. Ch. 5, Analog transmission, p. 146–148. ISBN: 978-0-07-296775-3

[3] LANCASTER, D. Chirp - A new radar technique. *Electronics World*, 1965, p. 42–43, 59.

[4] WINKLER, M. Chirp signals for communications. *IEEE WESCON Convention Record*, 1962, vol. 14, no. 2.

[5] GOTT, G. F., NEWSOME, J. P. HF data transmission using chirp signals. *Proceedings of the Institution of Electrical Engineers,* 1971, vol. 118, no. 9, p. 1162–1166. DOI: 10.1049/piee.1971.0210

[6] REYNDERS, B., POLLIN, S. Chirp spread spectrum as a modulation technique for long range communication. In *2016 Symposium on Communications and Vehicular Technologies (SCVT)*. Mons (Belgium), 2016, p. 1–5. DOI: 10.1109/SCVT.2016.7797659

[7] ROY, R., LOWENSCHUSS, O. Chirp waveform generation using digital samples. *IEEE Transactions on Aerospace and Electronic Systems*, 1974, vol. 10, no. 1, p. 10–16. DOI: 10.1109/TAES.1974.307958

[8] GONZALEZ, J. E., PARDO, J. M., ASENSIO, A., et al. Digital signal generation for LPM-LPI radars. *Electronics Letter*, 2003, vol. 39, no. 5, p. 464–465. DOI: 10.1049/el:20030316

[9] PUZYREV, P. I., KVACHEV, M. A., EROKHIN, V. V. Frequency shift chirp modulation with additional differential phase shift keying. In *2019 20th International Conference of Young Specialists on Micro/Nanotechnologies and Electron Devices (EDM)*. Erlagol (Russia), 2019, p. 78–82. DOI: 10.1109/EDM.2019.8823174

[10] HANIF, M., NGUYEN, H. H. Frequency-shift chirp spread spectrum communications with index modulation. *IEEE Internet of Things Journal*, 2021, vol. 8, no. 24, p. 17611–17621. DOI: 10.1109/jiot.2021.3081703

[11] GRETINGER, M., SECARA, M., FESTILA, CL., et al. Chirp signal generators for frequency response experiments. In *2014 IEEE International Conference on Automation, Quality and Testing, Robotics.* Cluj-Napoca (Romania), 2014, p. 1–4. DOI: 10.1109/AQTR.2014.6857860

[12] TELKAMP, T. LoRa, LoRaWAN, and the challenges of long-range networking in shared spectrum. *Cognitive Radio Platform NL*, 2015.

[13] LEE, G., PARK, W., KANG, T., et al. Chirp-based FHSS receiver with recursive symbol synchronization for underwater acoustic communication. *Sensors,* 2018, vol. 18, no. 12, p. 1–18. DOI: 10.3390/s18124498

[14] NAMIAS, V. The fractional order Fourier transform and its application to quantum mechanics. *IMA Journal of Applied Mathematics*, 1980, vol. 25, no. 3, p. 241–265. DOI: 10.1093/imamat/25.3.241

[15] ALMEIDA, L. B. The fractional Fourier transform and time-frequency representations. *IEEE Transactions on Signal Processing*, 1994, vol. 42, no. 11, p. 3084–3091. DOI: 10.1109/78.330368

[16] OZAKTAS, H. M., ARIKAN, O., KUTAY, M. A., et al. Digital computation of the fractional Fourier transform. *IEEE Transactions on Signal Processing*, 1996, vol. 44, no. 9, p. 2141–2150. DOI: 10.1109/78.536672

[17] SFORZA, F. (NANOSCALE LABS). *Communications System*. US patent US 8.406.275 B2, 2013.

[18] HISCOCK, P. D. (CAMBRIDGE SILICON RADIO LIMITED) *Chirp Communications*. US Patent US 8.718.117 B2, 2014.

[19] GOURSAUD, C., GORCE, J. M. Dedicated networks for IoT: PHY/MAC state of the art and challenges. *EAI Endorsed Transactions on Internet of Things*, 2015, vol. 1, no. 1, p. 1–11. DOI: 10.4108/eai.26-10-2015.150597

[20] SPRINGER, A., GUGLER, W., HUEMER, M., et al. Spread spectrum communications using chirp signals. In *IEEE/AFCEA EUROCOMM 2000. Information Systems for Enhanced Public Safety and Security*. Munich (Germany), 2000, p. 166–170. DOI: 10.1109/EURCOM.2000.874794

[21] MROUE, H., NASSER, A., PARREIN, B., et al. Analytical and simulation study for LoRa modulation. In *2018 25th International Conference on Telecommunication (ICT).* Saint-Malo (France), 2018, p. 655–659. DOI: 10.1109/ICT.2018.8464879

[22] BOYLESTAD, R. L., NASHELSKY, L. *Electronic Devices and Circuit Theory.* 11th ed. New York (USA): Pearson, 2012. Ch. Diode applications. p. 78–91. ISBN: 978-0132622264

[23] KLAUDER, J. R., PRICE, A. C., DARLINGTON, S., et al. The theory and design of chirp radars. *Bell System Technical Journal*, 1960, vol. 39, no. 4, p. 745–808. DOI: 10.1002/j.1538-7305.1960.tb03942.x

[24] ALSHAREF, M. A. Constant-envelope multi-level chirp modulation: Properties, receivers, and performance. *Ph.D. Thesis.* Dept. Electrical and Computer Eng., Univ. of Western Ontario, (Ontario, Canada), 2016.

[25] ALSHAREF, M., HAMED, A., RAO, R. K. Error rate performance of digital chirp communication system over fading channels. In *Proceedings of the World Congress on Engineering and Computer Science (WCECS 2015).* San Francisco (USA), 2015, [Online] Available at: http://www.iaeng.org/ WCECS2015

[26] PROAKIS, J. G., SALEHI, M. *Digital Communications.* 5th ed. New York (USA): McGraw-Hill, 2008. Ch. 13, Fading channels I: Characterization and signaling, p. 830–898. ISBN: 978–0–07–295716–7

[27] KAMINSKY, J., SIMANJUNTAK, L. Chirp slope keying for underwater communications. In *Proceedings of SPIE Sensors, and Command, Control, Communications, and Intelligence (C31) Technologies for Homeland Security and Homeland Defense IV Conference.* Orlando (FL, USA), 2005, vol. 5778, p. 894–905. DOI: 10.1117/12.605426

About the Authors …

Lerson KIRASAMUTHRANON received B.Eng, M.S. degree in Telecommunication Engineering and D.Eng. degree in Electrical Engineering from King Mongkut's Institute of Technology Ladkrabang (KMITL), Bangkok, Thailand, in 2009, 2012 and 2016, respectively. His research interests include analog circuits in telecommunication systems and digital signal processing.

Paramote WARDKEIN received his M.E.and D.Eng. degree in Electrical Engineering from King Mongkut's Institute of Technology Ladkrabang (KMITL), Bangkok, Thailand, in 1990 and 1997, respectively. He is now an Associate Professor of Telecommunications Engineering Department, Faculty of Engineering, (KMITL), Thailand. His research interests include analog circuits in telecommunication systems and digital signal processing.

Jeerasuda KOSEEYAPORN graduated M.S. and Ph.D. degrees in Electrical Engineering from Vanderbilt University, Nashville, TN, USA, in 1999 and 2003, respectively. Currently, she is an Associate Professor of Telecommunications Engineering Department, Faculty of Engineering, (KMITL), Thailand. The research interests are in the areas of analog circuits in telecommunication systems and digital signal processing.